Supplementary information (Figures and Text)

Figure S1: Spinel-V_2O_3 textures in 1400 °C experimental samples

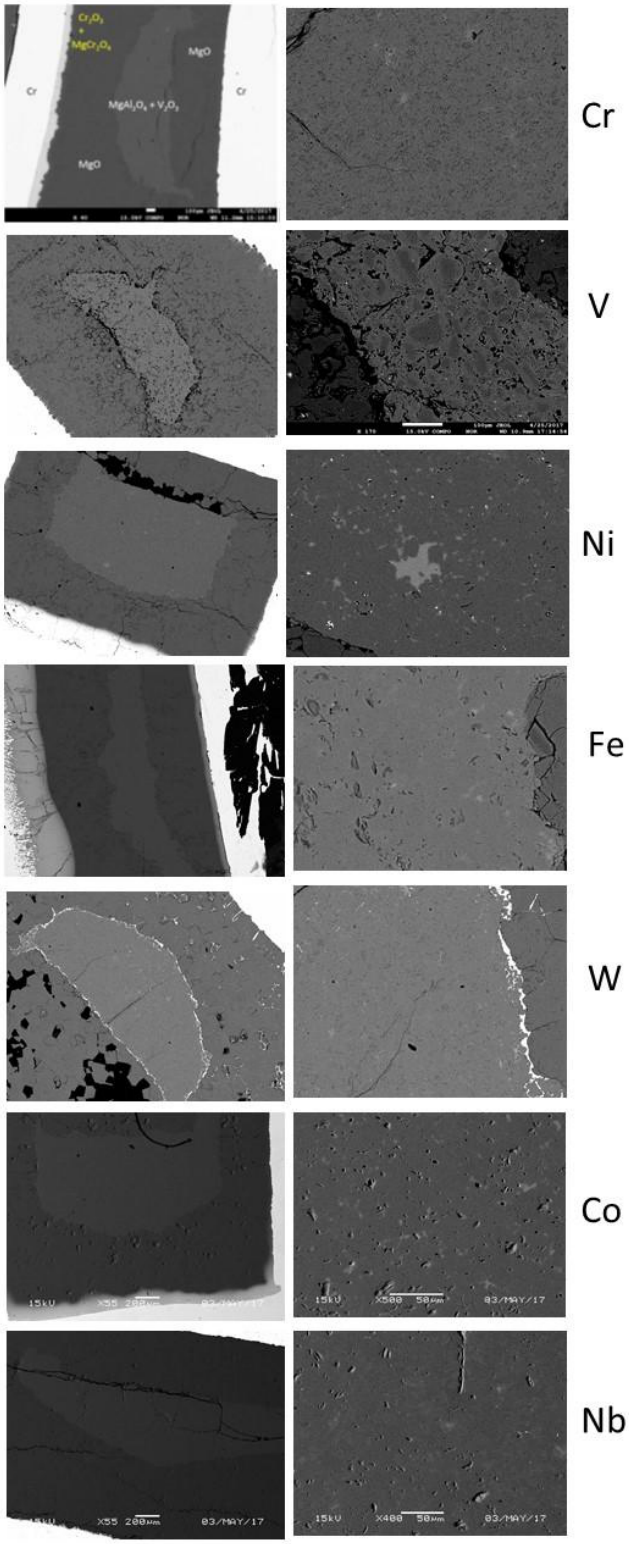

Figure S2: Comparison of V-*K* edge spectra from magnesiospinel formed at IW-5.44 (experiment V-008) with V_2O_3. V_2O_3 spectrum reproduced from the EXAFS spectral library and was acquired at the Advanced Photon Source: https://xaslib.xrayabsorption.org/rawfile/235).

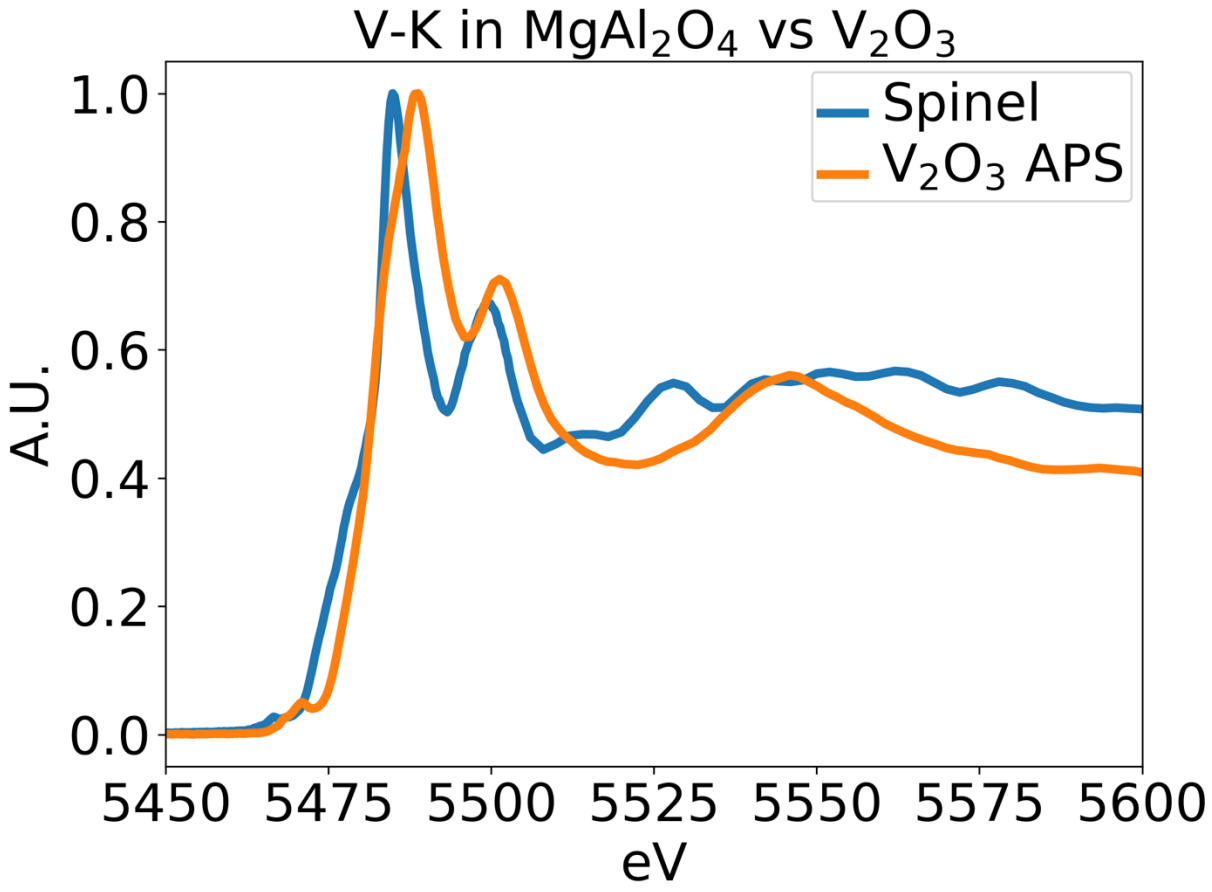

Figure S3: 1400 °C spinel V XANES *K* edge spectra

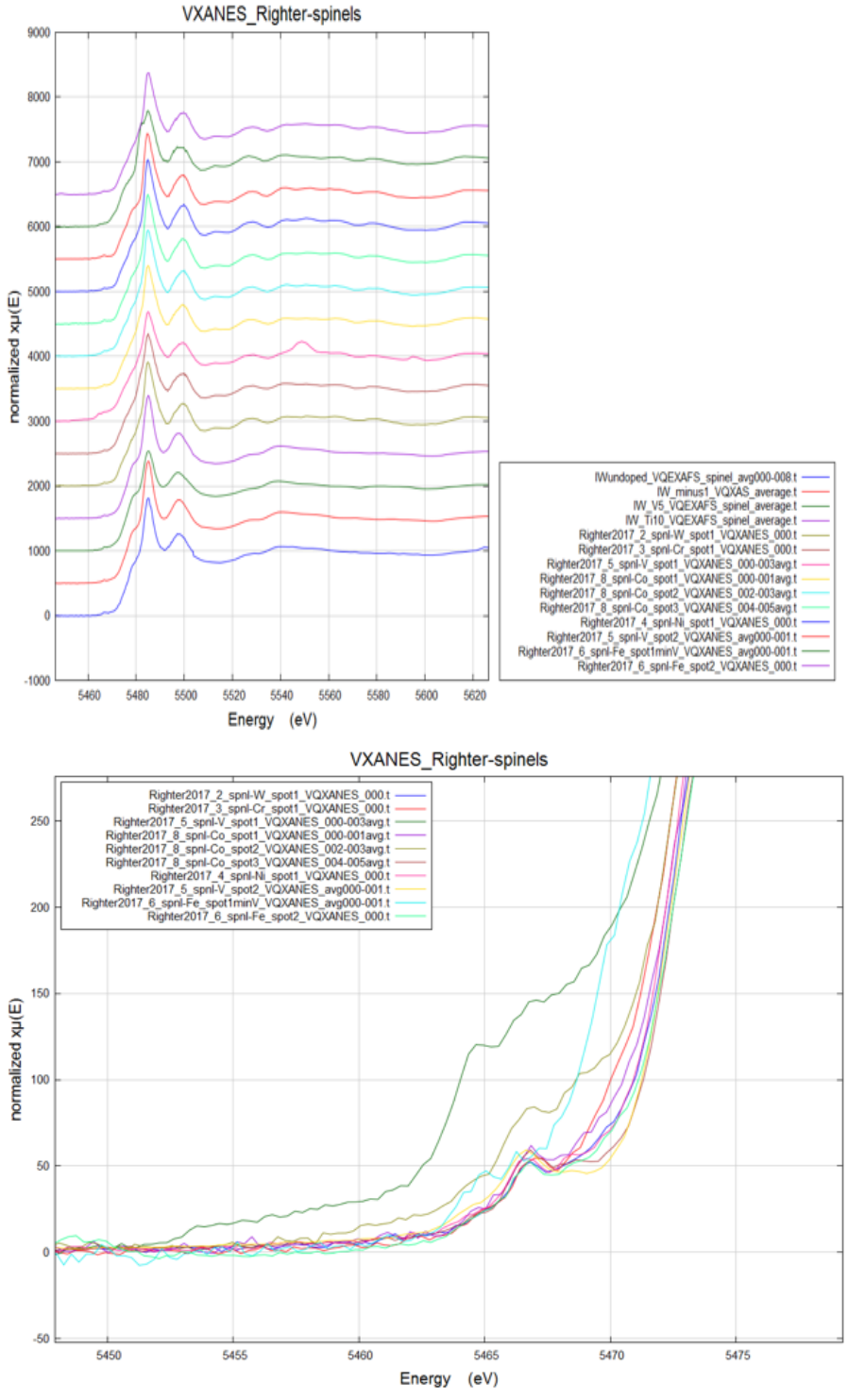

Supplementary text

Part 1: An example of verifying V in spinel using the Spinel-V-008 TEM analysis.

Samples used for calibration of the V barometer were verified as V-bearing spinels using the following criteria: (a) equilibrated, (b) contained spinel, and (c) that the V was present within the spinel crystal structure. We discuss solutions to (a) in other portions of the paper (see discussion of equilibration in the Experimental Methods section of the main text of the manuscript).

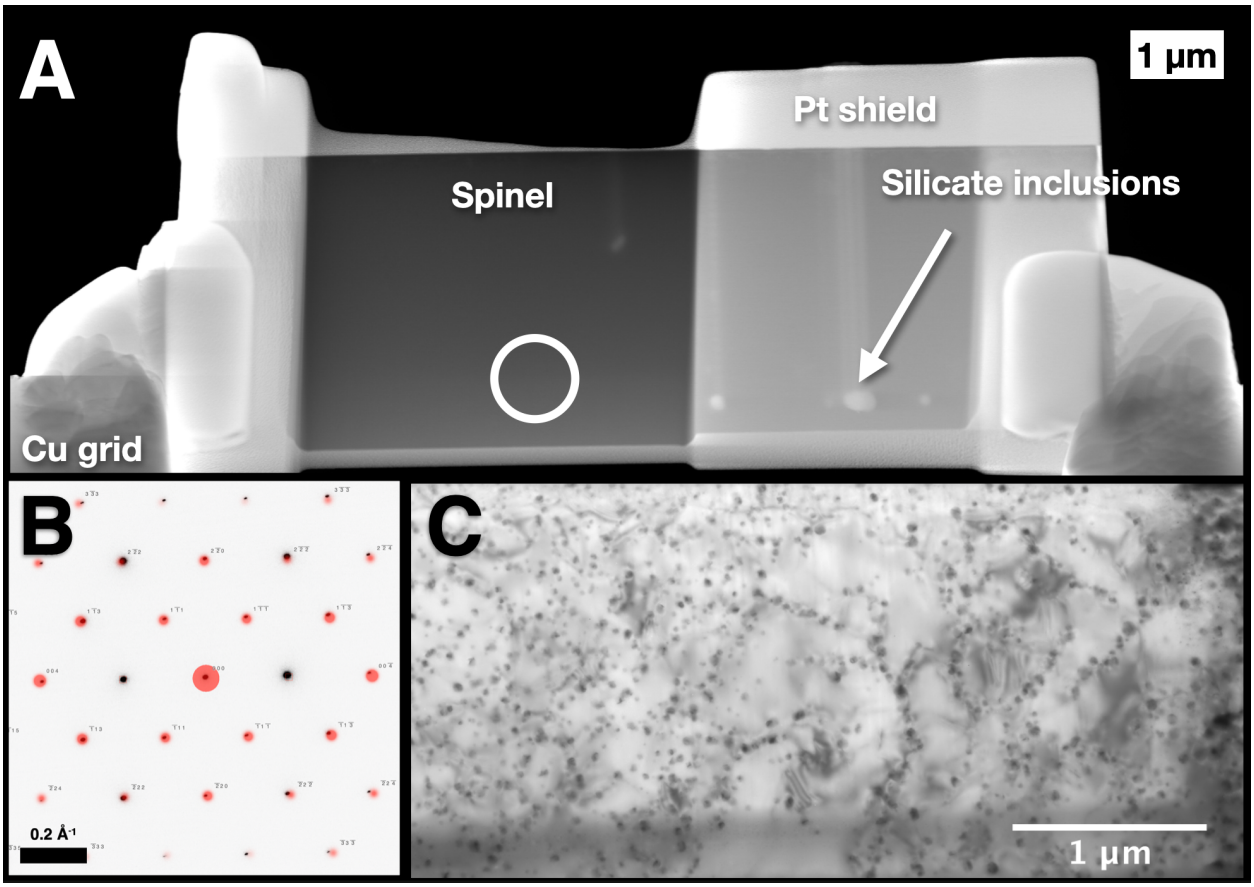

Figure S4: (A) STEM image of Spinel V-008 FIB section. The bulk of the material is spinel. A few silicate inclusions that do not contain V are also visible. (B) Selected area diffraction pattern of the [110] zone axis pattern for spinel. The diffraction was taken from the region marked with the circle in A. Black dots are the measured reflections and red spots are calculated kinematical reflections. (C) Sample 2016,2 - Ti-Spnl-3, which contains Ti-V metal nanoparticles and demonstrates that this sample was not satisfactory for V-XANES analysis.

To verify the presence of spinel in key samples, FIB sections were extracted and studied using the TEM. **Figure S4A** shows a FIB section from spinel V-008 equilibrated at $\log(f_{O2})$ = IW-5.44

and 1600 °C. Spinel crystal structures were verified using selected area electron diffraction. The diffraction pattern can be seen in **Figure S4B** along with a theoretical simulation of the diffraction pattern (Palmer, 2015). It indexes to the [110] zone axis. Two forbidden reflections are present because of dynamical diffraction, and no additional reflections from unverified phases are present. An EDS spectrum was acquired off zone axis, or in the case of spinel V-008 while rocking the electron beam around zone [110] by ½ nm^{-1} (ALCHEMI; Jones, 2003) in order to average over electron scattering effects for an unbiased quantification. EDS spectra had enough counts to verify that V was present in the same abundance seen by the microprobe, i.e. 1272 ppm V_2O_3. In addition, ALCHEMI patterns verified that Mg and Al were in the tetrahedral and octahedral sites of spinel, respectively. V was clearly visible in the aggregate ALCHEMI spectrum, but the ALCHEMI images were too noisy to verify which site the V resides in. Therefore, only the analysis of XANES and EXAFS spectra were used to verify that the V resides in the octahedral site. As noted in the theoretical section of the paper, octahedral and tetrahedral V have dramatically different near edge structure and are easily distinguished.

Because TEM is able to image down to the atomic scale, V is demonstrably present within the spinel structure and not present, e.g. as small nanometal inclusions. In cases where equilibrium was not reached or did not favor V residing in spinel, TEM did show small nanometal inclusions, or significant distribution of V into other phases. For example, **Figure S4C** shows a spinel containing Ti-V nanometal inclusions from sample 2016,2 Ti-Spnl-3 (1400 °C, 1 GPa, 6 hrs). This sample is not included in the current study, because the TEM results showed that the V did not reside in the spinel but rather in the Ti-V nanometal inclusions.

Another issue that could arise is whether the synchrotron probe extracted a spectrum from the exact same region as the TEM analysis. To ensure this link was robust, the following sequence was used:

- Microprobe analysis was first acquired to verify the spinel composition, ensure the sample was a good candidate with large spinels > 10 microns across, and demonstrate equilibration with V in the spinel. It is necessary to have a large spinel in order that the excitation volume of the microprobe and synchrotron beams measure only the spinel and no other phases beneath.

- After microprobe analysis was complete, higher resolution SEM images of candidate regions were acquired to search for and rule out problematic inclusions in the spinel that may not have been visible at the microprobe's resolution. Then EDS maps of the candidate spinel were acquired to ensure that there was no subsurface heterogeneity within the volume we wanted to study. Specifically, we looked for at least 10 μm diameter patches of spinel where the composition was homogenous.
- Once candidate regions were chosen, the same region was also mapped in the synchrotron using a photon energy above the V-K edge and verified that the chosen region was heterogeneous. Because the penetration depth of X-ray photons can be large, it is not always true that a sample that looks homogenous in the SEM is homogenous in the synchrotron. Once this was verified, XANES was acquired next. In some cases, we found impurities or other potentially interesting V-bearing phases that were not spinel, so some XANES spectra intentionally sample these. They are mentioned where appropriate in the paper.
- Once the synchrotron work was finished, we FIBed the exact spot measured in the synchrotron and verified it using TEM.

Spinel V-008 is the definitive low fugacity, equilibrated sample and the full verified analytical chain described above was applied to it. TEM analysis was not done on every sample since TEM analysis is very time consuming. However, all samples received full consideration of excitation volumes in the SEM and synchrotron.

Part 2: CMAS glass interpretation

The suite of CMAS glasses showed a poor correlation between V K pre-edge peak intensity and log fO_2 of the buffer (**Fig. S5**). This could be due to several factors, including: pressure effect on the pre-edge peak intensity, quench rate of the experiments, glass compositional variation, extrapolation outside of the calibration range, and possible beam damage effects.

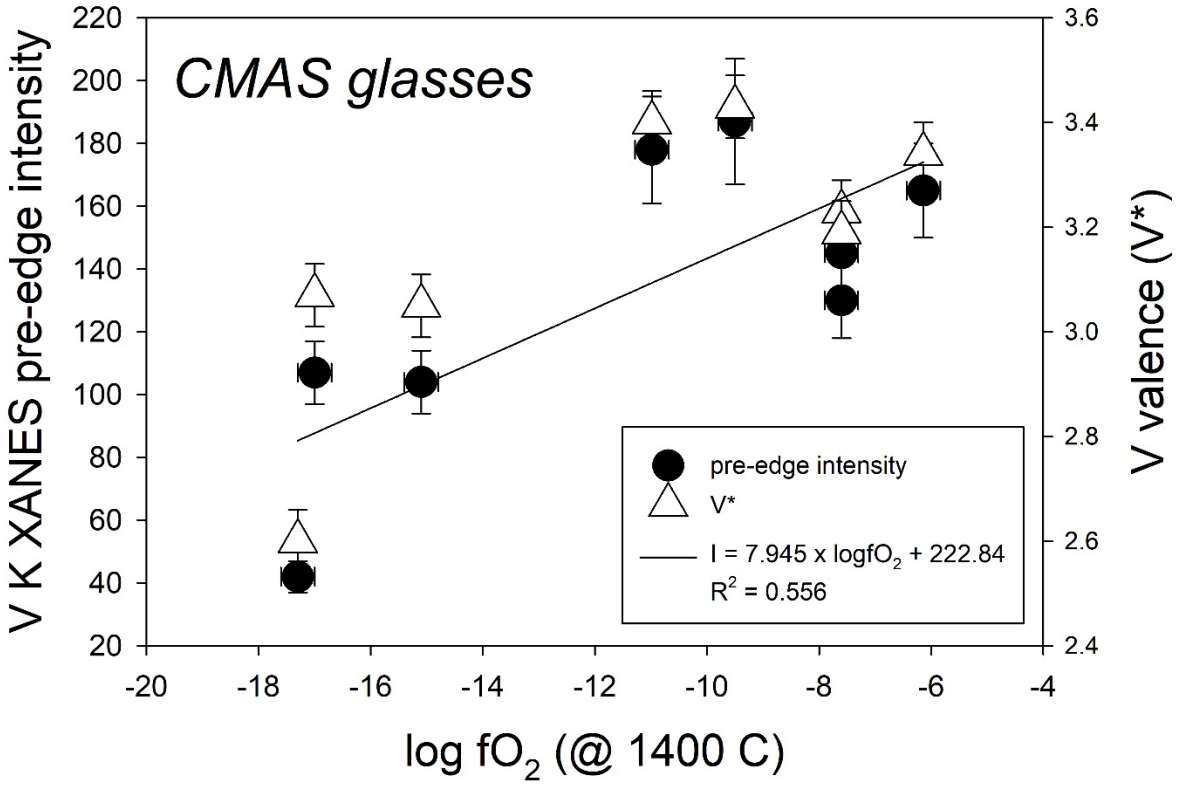

Figure S5: V K XANES pre-edge intensity (circles) and V* valence (triangles) versus log f_{O2} for our suite of CMAS glasses. Also shown is a linear fit to the pre-edge intensity data showing the $R^2 = 0.556$. All glasses were equilibrated at 1400 °C (IW is at -10) with V pre-edge peak intensity and V* valence calculated using the Sutton et al. (2005) experiments on CMAS system at 1400 °C. V* of Sutton et al. (2005): $I = -153 + 199(V^*) - 106(V^*)^2 + 2.4(V^*)^3$.

Pressure: The V XANES oxybarometer of Sutton et al. (2005) was calibrated on glasses synthesized at 0.1 MPa conditions, yet we have applied it here to glasses from 1.0 GPa. Experimental glasses produced at 1.8 and 1.85 GPa experiments from Righter et al. (2011) exhibit a slightly lower V* than similar glasses synthesized at 0.1 MPa by Righter et al. (2006) (**Fig. S6**). This difference is small and still overlapping the values of V* measured in the 0.1 MPa glass suite indicating that this effect might be small to negligible. Furthermore, any pressure effect that would be evident in our 1.0 GPa glasses should be systematically lower for all glasses, which is not consistent with the scatter seen in our data. It seems that pressure effects are not responsible for the poor correlation.

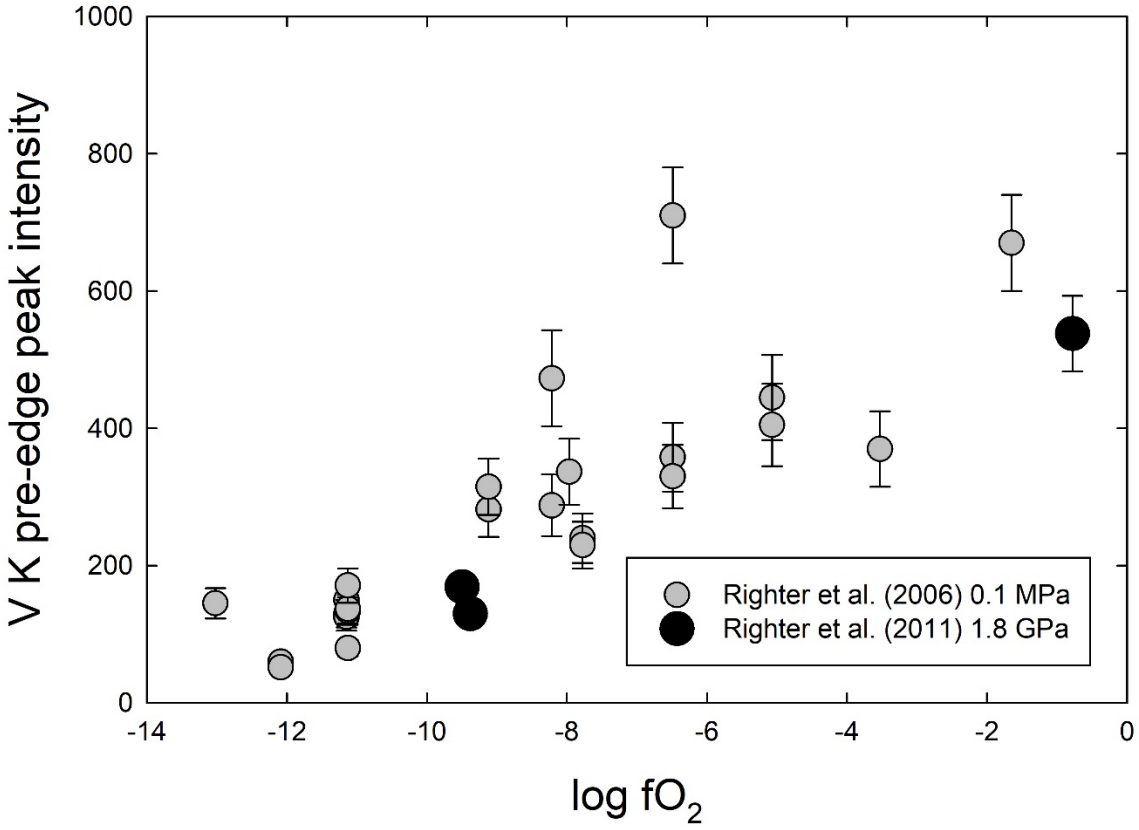

Figure S6: V *K* XANES pre-edge intensity versus log f_{O2} for 0.1 MPa glasses from Righter et al. (2006) (grey circles) compared to 1.8 and 1.85 GPa glasses from Righter et al. (2011). The latter plot at the lower end edge of the data for 0.1 MPa data suggesting a small, if any, pressure effect on pre-edge intensity. These sparse data should be taken as motivation for future work and the interpretation is speculative.

Quench effects: The quench conditions were rapid, and typically for this sample assembly and piston cylinder apparatus, temperatures drop to 100 to 200 °C within 2 or 3 seconds. We have added this information to this section so that the reader knows this is a rapid quench, not a slow one. These rapid quench rates will avoid the complications of cooling near the glass-forming temperature. This has also recently been discussed and explained by Mare et al. (2021) with respect to Ga and Ge in glasses. The work of Berry shows that changes in Cr redox state can be induced during quench by coupled equilibria involving Fe: $Cr^{3+} + Fe^{2+} = Cr^{2+} + Fe^{3+}$. Several other elements have exhibited no differences between valence measured in annealing at glass transformation temperature and quenching in glass composition that are Fe-free, such as Ge and Ga (Mare et al., 2021). Since we have no Fe in our glasses, and the quench rate was rapid, V in our glasses should be free of valence modifying quenching effects.

Glass compositional variation: The careful work of Sutton et al. (2005) highlighted the dependence of pre-edge peak intensity on some glass bulk compositional features such as Ti content. Addition of 5% TiO_2 to glasses can result in reduction of pre-edge peak intensity - shifted to lower intensities by 50 units. Dependencies of pre-edge peak intensity on glass composition has also been observed in Cr valence studies with Ti-bearing glasses (Bell et al., 2020). If small concentrations of transition element oxides dissolved into the glass of interest can cause reduction of pre-edge peak intensities of this magnitude, then such an effect may have influenced some of the glasses in our work. The Ni-NiO and Co-CoO buffered experiments also contain ~ 5 wt% WO_3 which may have influenced the pre-edge peak intensities. Pre-edge peaks from both of these oxidized glasses were lower than expected. Similarly, the Mo-MoO_3 buffered experiments contained ~7 wt% MoO_3, which also may have influenced the pre-edge peak intensities. This is speculative, but might be a subtle effect that has gone unrecognized. Additionally, there are small variations in the bulk glass compositions that could also have imparted some scatter into the glass database. In summary, compositional variation in the glasses could have contributed to the sub-optimal correlation seen in our glass suite.

Oxybarometer calibration range: The Sutton oxybarometer was calibrated on a suite of low Ti glasses equilibrated at 1400 °C within a specific logfO_2 range from -8 to -13.3 (**Fig. S7**). At lower logf_{O2} values the pre-edge peak intensities do not continue to fall with decreasing logf_{O2} – instead they flatten out as noted by the authors with some discussion as to why. Our lowest logf_{O2} glasses fall below the calibration range and within this reduced glass region where there is uncertainty about pre-edge peak intensities. The inherent uncertainty in this reduced glass region is also a contributing factor to the sub-optimal correlation seen in our glass suite.

Beam damage from high photon flux densities: Some recent studies have shown that Fe, S, and V pre-edge peak intensities in hydrous glasses and oxidized glasses can be susceptible to beam damage, and the damage is enhanced at high photon flux densities (Cottrell et al., 2018; Head et al., 2018; Lanzirotti et al., 2022; Lerner et al., 2021). Lanzirotti et al., 2022, in particular, showed that V pre-edge peak intensities can be reduced by high flux beam damage, leading to erroneously low valence determinations. Although this might be a concern in our oxidized glasses (NNO and

CCO), which yield lower than expected pre-edge peaks and valences, the photon flux densities we utilized are lower than where this effect has been documented. The photon flux density at ALS Beamline 10.3.2 is from $3x10^7$ to 10^8 photons/s/μm^2 for our measurements, given the maximum flux at 6 keV is 10^9 photons/s, and our V XANES data were acquired with the beam attenuated by slits to achieve high energy resolution. These flux densities are much lower than the threshold value suggested by Lanzirotti et al. (2022) of < $1x10^9$ photons/s/μm^2. Therefore, it is unlikely that beam damage has played a role in the sub-optimal correlation seen in our glass suite.

In summary, the effect of glass compositional variation, coupled with extrapolation outside of the calibrated oxybarometer range have both likely contributed to the poor correlation seen in our glass suite. On the other hand, pressure effects, quench effects, and beam damage did not play a significant role in the correlation. We have described these effects here in some detail so that others might take these lessons learned and apply them to future efforts to expand the applicability of the V XANES oxybarometer for glasses.

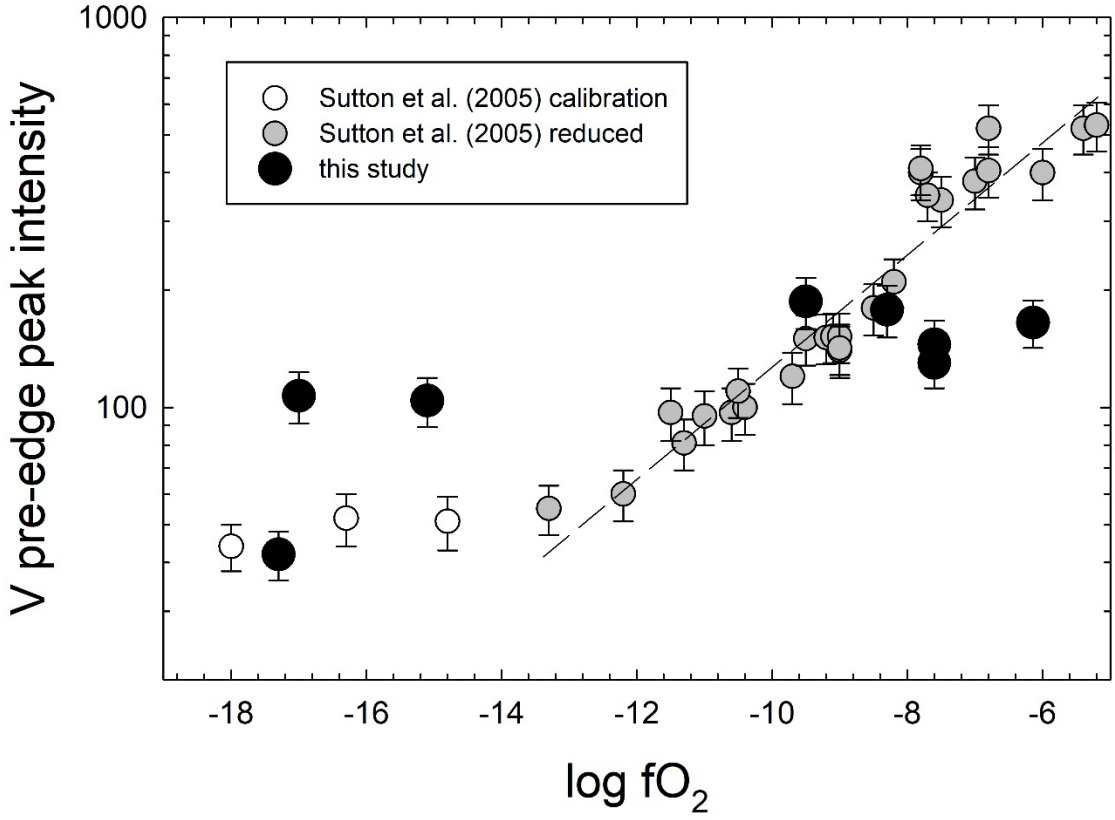

Figure S7: V *K* XANES pre-edge intensity versus logf_{O2} for 0.1 MPa glasses from Sutton et al. (2005). The low Ti glass dataset used for their oxybarometer calibration is shown as grey circles, while the reduced glasses not included in the calibration are shown as open circles. Data from this study are shown as black circles.

Supplementary Text references:

Bell, A. S., Vaci, Z., Lanzirotti, A. (2021) An Experimental-XANES Investigation of Cr Valence Systematics in Basaltic Liquids and Applications to Modeling $Cr^{2+}/\Sigma Cr$ Evolution in Crystallizing Basaltic Magma Systems. *Geochimica et Cosmochimica Acta 292*, 130-151.

Berry, A. J., Shelley, J. M. G., Foran, G. J., O'Neill, H. S. C., Scott, D. R. (2003) A furnace design for XANES spectroscopy of silicate melts under controlled oxygen fugacities and temperatures to 1773 K. *Journal of synchrotron radiation 10*, 332-336.

Cottrell, E., Lanzirotti, A., Mysen, B., Birner, S., Kelley, K.A., Botcharnikov, R., Davis, F.A. and Newville, M. (2018) A Mössbauer-based XANES calibration for hydrous basalt glasses reveals radiation-induced oxidation of Fe. *American Mineralogist: Journal of Earth and Planetary Materials 103*, 489-501.

Head, E., Lanzirotti, A., Newville, M., Sutton, S. (2018) Vanadium, sulfur, and iron valences in melt inclusions as a window into magmatic processes: A case study at Nyamuragira volcano, Africa. *Geochimica et Cosmochimica Acta 226*, 149-173.

Jones, I. P. (2003) Determining the locations of chemical species in ordered compounds: ALCHEMI. *Advances in imaging and electron physics* **125**, 63–I.

Lanzirotti, A., Sutton, S.R., Newville, M., and Head, E.S. (2022) Radiation-induced changes in Vanadium speciation in basaltic glasses: implications for oxybarometry measurements using Vanadium K-edge X-ray absorption spectroscopy. American Mineralogist, in press.

Lerner, A.H., Muth, M.J., Wallace, P.J., Lanzirotti, A., Newville, M., Gaetani, G.A., Chowdhury, P. and Dasgupta, R. (2021) Improving the reliability of Fe-and S-XANES measurements in silicate glasses: correcting beam damage and identifying Fe-oxide nanolites in hydrous and anhydrous melt inclusions. *Chemical Geology*, p.120610.

Mare, E. R., O'Neill, H. S. C., Berry, A. J., Frigo, C., Glover, C. J. (2021) Coordination change of Ge^{4+} and Ga^{3+} in silicate melt with pressure. *Geochimica et Cosmochimica Acta 303*, 184-204.

Palmer, D. C. (2015) Visualization and analysis of crystal structures using CrystalMaker software. *Zeitschrift Für Kristallographie - Cryst Mater* **230**, 559–572.

Righter, K., Sutton, S.R., Newville, M., Le, L., Schwandt, C.S., Uchida, H., ... and Downs, R.T. (2006) An experimental study of the oxidation state of vanadium in spinel and basaltic melt with implications for the origin of planetary basalt. American Mineralogist, 91, 1643-1656.

Righter, K., Sutton, S., Danielson, L., Pando, K., Schmidt, G., Yang, H., Berthet, S., Newville, M., Choi, Y., Downs, R.T. and Malavergne, V. (2011) The effect of fO_2 on the partitioning and valence of V and Cr in garnet/melt pairs and the relation to terrestrial mantle V and Cr content. *American Mineralogist 96*, 1278-1290.

Sutton, S.R., Karner, J., Papike, J.J., Delaney, J.S., Shearer, C., Newville, M., ... and Dyar, M.D. (2005) Vanadium K edge XANES of synthetic and natural basaltic glasses and application to microscale oxygen barometry. Geochimica et Cosmochimica Acta, 69, 2333-2348.